Published in final edited form as:
J Chem Theory Comput. 2012 December 11; 8(12): . doi:10.1021/ct300758v.

Fragment-based Quantum Mechanical/Molecular Mechanical Simulations of Thermodynamic and Kinetic Process of the Ru^{2+}–Ru^{3+} Self-Exchange Electron Transfer

Xiancheng Zeng[a], **Xiangqian Hu**[a], and **Weitao Yang**[*,a,b]

[a]Department of Chemistry, Duke University, Durham, NC 27708, USA

[b]Department of Physics, Faculty of Science, King Abdulaziz University, P.O. Box 80203, Jeddah 21589, Saudi Arabia

Abstract

A fragment-based fractional number of electron (FNE) approach, is developed to study entire electron transfer (ET) processes from the electron donor region to the acceptor region in condensed phase. Both regions are described by the density-fragment interaction (DFI) method while FNE as an efficient ET order parameter is applied to simulate the electron transfer process. In association with the QM/MM energy expression, the DFI-FNE method is demonstrated to describe ET processes robustly with the Ru^{2+}-Ru^{3+} self-exchange ET as a proof-of-concept example. This method allows for systematic calculations of redox free energies, reorganization energies, and electronic couplings, and the absolute ET rate constants within the Marcus regime.

1. Introduction

Electron transfer (ET) process is one of the fundamental processes in chemistry, biochemistry, and material science.[1] The Marcus theory for electron transfer characterizes the ET rate constant as,[2]

$$k_{ET}=\frac{2\pi}{\hbar}\frac{1}{\sqrt{4\pi\lambda k_B T}}\left\langle H_{DA}^2\right\rangle \exp\left(-\frac{(\Delta G+\lambda)^2}{4\lambda k_B T}\right), \quad (1)$$

where H_{DA} is the donor-acceptor electronic coupling, the symbol <…> denotes the thermal average, λ is the reorganization energy, ΔG is the ET reaction free energy, k_B is Boltzmann's constant, and T is the temperature (298K in this work). Although the Marcus theory is semiclassical and is based on transition-state theory, which assumes weak coupling and slow solvation limit,[3] it has been applied successfully to elucidate and compute the ET rate constants for many chemical systems.[4-7] As such, accurate calculations of each term in eq. 1 are pivotal to facilitate the understanding of the ET process with atomistic and electronic details. To calculate the parameters, e.g. $<H^2_{DA}>$, ΔG, and λ, for ET processes, many methods have been developed using empirical,[8,9] semiclassical or quantum mechanical

*Corresponding Author: weitao.yang@duke.edu.

Author Contributions: The manuscript was written through contributions of all authors. All authors have given approval to the final version of the manuscript.

Notes: The authors declare no competing financial interest.

Supporting Information: Figure. S1, S2, S3 and Table S1, S2, S3. This material is available free of charge via the Internet at http://pubs.acs.org.

models,[10-18] and classical[19-24] or density functional based MD simulations.[25-47] A more detailed discussion of these works is beyond the scope of this work but has been summarized in a number of reviews.[48-55] We note that only few practical *ab initio* method,[37,43] using constrained density functional theory (DFT)[56] or time dependent DFT, have been proposed to systematically compute the key terms: $\langle H^2_{DA} \rangle$, ΔG, λ, and the final ET rate constant. Usually, these terms are calculated using different schemes. For instance, to obtain the ensemble average of H^2_{DA}, classical molecular mechanical (MM) molecular dynamics (MD) simulations are frequently performed to explore the conformational ensemble of either the product or reactant state, without sampling the adiabatic ET transition state. For ΔG and λ, methods using a combination of QM treatment and continuum model have been commonly employed to approximate the explicit environments, but they inevitably miss some details of the environments, including entropic, dynamic and conformational contributions, which are especially important for protein systems.[18,27] In order to reach a theoretical estimation of k_{ET}, one must combine various schemes, and ensure each scheme can yield results directly comparable to experiments. Therefore, developing a systematic method is still important for understanding the microscopic kinetics, thermodynamics, and mechanism of ET processes at the atomistic and electronic level.

A challenging task for theoretical simulations on k_{ET} is how to balance the computational cost and accuracy. The hybrid quantum mechanical and molecular mechanical (QM/MM) method becomes a very promising tool to simulate the ET process: QM describes the region involving electron transfer while the rest of the system is simulated by MM. In our previous work, we demonstrated that using the fractional number of electron (FNE) as the order parameter in the "on-the-fly" QM/MM simulations,[57] the redox potential residing in ΔG could be computed accurately and the ET half reaction processes could be characterized as well. When combined with the QM/MM minimum free energy path (MFEP) method,[58,59] the resulted QM/MM-MFEP/FNE can simulate the ET half reactions for organic molecules and proteins because of the efficiency gained.[60] However, the FNE approach has been limited to study of the ET half reaction rather than the entire ET process from the electron donor region to the acceptor region. As such, the electronic coupling term or reorganization energy term of ET cannot be computed readily using FNE.

In this work, we combine the density-fragment interaction (DFI) method with FNE (i.e., DFI-FNE) to simulate the entire ET transfer process in association with "on-the-fly" QM/MM simulations. DFI method, based on the Kohn-Sham density functional theory (KS-DFT), was originally developed to achieve the linear scaling of computational cost with respect to the growing system size.[61] In particular, we reformulated DFI to reduce the computational cost and make it applicable for large molecular systems.[62] For instance, we demonstrated that our new DFI method can simulate the thermodynamic properties of liquid water efficiently and accurately. DFI is essentially the simplest divide-and-conquer (DAC)[63,64] method without any buffer region, but with frozen fragment pseudopotentials. In DFI, the entire QM system is first divided into small fragments, then each fragment is computed independently, and the desired properties of the entire system are evaluated using the solved fragment information. Interestingly, the fragmentation process can be viewed as the electron localization step. For each fragment in DFI, the number of electrons is fixed and localized in its own region. Therefore, we can gradually move one electron from one fragment to another fragment using FNE as the order parameter to simulate the entire ET process while the environment can be simulated by MM.

This paper is organized as follows. We first briefly review the DFI and FNE approaches and introduce the combined DFI-FNE QM/MM scheme for ET simulations. In Sec. 3, we show the computational details of our simulations on the Ru^{2+}–Ru^{3+} self-exchange ET process in

aqueous solution as a simple but essential testing case. In Sec. 4, we elucidate how to compute $\langle H^2_{DA} \rangle$, ΔG, and λ to obtain k_{ET} and discuss some challenging issues related to the accuracy. Finally, we conclude our work in Sec. 5.

2. Methods

2.1 Density Fragment Interaction (DFI) Approach

Briefly, we reformulated the DFI energy expression as,

$$E[\rho] = \sum_{i=1}^{N_F} E_i^F[\rho_i] + E_{ESP}^{FF}[\{\rho_i\}]. \quad (2)$$

Here, $\rho(\mathbf{r}) = \sum_{\mathbf{i}=\mathbf{1}}^{\mathbf{N_F}} \rho_{\mathbf{i}}(\mathbf{r})$ and ρ_i is the electron density of fragment *i*. $E_i^F[\rho_i]$ is the self-energy of fragment *i*,

$$E_i^F[\rho_i] = T_s[\rho_i] + \int V_i(\mathbf{r})\rho_{\mathbf{i}}(\mathbf{r})\mathbf{dr} - \int \sum_{\mathbf{j}\neq\mathbf{i}}^{\mathbf{N_F}} \mathbf{V}_{\mathbf{j}}^{ESP}(\mathbf{r})\rho_{\mathbf{i}}(\mathbf{r})\mathbf{dr} + \int \sum_{\mathbf{j}\neq\mathbf{i}}^{\mathbf{N_F}} \mathbf{V}_{\mathbf{j}}^{FFP}(\mathbf{r})\rho_{\mathbf{i}}(\mathbf{r})\mathbf{dr} + \mathbf{J}[\rho_{\mathbf{i}}] + \mathbf{E}_{xc}[\rho_{\mathbf{i}}] + \mathbf{E}_{NN}^{\mathbf{i}}. \quad (3)$$

$E_{ESP}^{FF}[\{\rho_i\}]$ is the electrostatic interaction energy between fragments,

$$E_{ESP}^{FF}[\{\rho_i\}] = \frac{1}{2}\sum_{i=1}^{N_F} \int \rho_i(\mathbf{r}) \sum_{\mathbf{j}\neq\mathbf{i}}^{\mathbf{N_F}} \mathbf{V}_{\mathbf{j}}^{ESP}(\mathbf{r})\mathbf{dr} + \frac{\mathbf{1}}{\mathbf{2}} \sum_{\mathbf{i}=\mathbf{1}}^{\mathbf{N_F}} \sum_{\mathbf{a}=\mathbf{1}}^{\mathbf{n_i}} \mathbf{Z}_{\mathbf{a}}^{\mathbf{i}} \sum_{\mathbf{j}\neq\mathbf{i}}^{\mathbf{N_F}} \mathbf{V}_{\mathbf{j}}^{ESP}(\mathbf{R}_{\mathbf{a}}^{\mathbf{i}}). \quad (4)$$

N_F is the number of fragments in the system and n_i is the number of atoms in fragment *i*. Z_a^i is the nucleic charge of atom *a* in fragment *i*, and $\mathbf{r}_a^i$ is the corresponding nucleic position. In our new DFI reformulations, we introduced $V_j^{FFP}(\mathbf{r})$, the frozen fragment pseudopotential for atom *j*, which takes the Pauli repulsive interactions among fragments into account and approximated $V_j^{FSP}(\mathbf{R}_a^i)$, using the simple ESP charges. Note that the frozen fragment pseudopotential depends on atomic type and needs to be fitted using a set of training molecules. In this work, we fitted the Pauli parameters for Ru, O, and H with BLYP/Lanl2dz using the fitting protocol described in Ref [62]. The finial parameters used in this work is listed in SI Table S1. Note that these parameters are negligible when the edge-edge distance between donor and acceptor groups is beyond 5 Å.[62]

2.2 Fractional Number of Electron (FNE) Approach

The FNE approach is illustrated in Fig. 1 for removing one electron from the electron donor group to simulate the ET half reaction,

$$A_{aq} \rightarrow A_{aq}^{+} + e^{-}. \quad (5)$$

Here, FNE is the order parameter to drive the system from one state to the other to achieve the sufficient sampling of free energy. In contrast to mix two potential energy functions to describe the transition from one state to the other,[28,29,31,33] FNE gradually changes the number of electrons in the system, which only requires one QM calculation for a given conformation. Fig. 1 shows that the number of electron on HOMO denoted by η is gradually

decreased from 1.0 to 0.0. According to the Janak theorem[65] and its extension to generalized Kohn-Sham calculations in our recent work,[57,66] the energy derivative with respect to the number of electron (expressed as the frontier occupation number) is

$$\frac{\partial E}{\partial \eta} = \varepsilon_{HOMO} \quad (6)$$

for both Kohn-Sham calculations with explicit density functionals and generalized Kohn-Sham calculations with orbital functional.[47,56] Thus, the free energy change (i.e., oxidation free energy) of eq. 5 can be readily computed by thermodynamic integration (TI),

$$\Delta A = -\int_0^1 \frac{\partial A(\eta)}{\partial \eta} d\eta = -\int_0^1 \left\langle \frac{\partial E(\eta)}{\partial \eta} \right\rangle_\eta d\eta = -\int_0^1 \langle \varepsilon_{HOMO} \rangle_\eta d\eta. \quad (7)$$

The FNE-TI approach has been applied successfully to compute the redox potential of metal ion in aqueous solution. In addition, the reorganization energy of the half reaction and activation free energy of the full reaction (assuming two reaction centers do not interact with each other) can be calculated by reusing the sampled trajectories using the energy gap *ΔE* as the reaction coordinate.[57]

2.3 Combined DFI-FNE QM/MM Simulations for Full ET Reactions

To simulate the realistic ET reaction process, the previous half reactions studied by FNE are not satisfactory since the electron must be driven from the donor to the acceptor to characterize the ET mechanism with both donor and acceptor groups present. Here, we combine the DFI method with FNE and TI to simulate the full ET process. In this work, we focus on using a simple ET reaction of Ru^{3+} and Ru^{2+} self-exchange in aqueous solution to demonstrate how DFI-FNE works,

$$\mathrm{Ru}_D^{2+}(H_2O)_6 + \mathrm{Ru}_A^{3+}(H_2O)_6 \rightarrow \mathrm{Ru}_D^{3+}(H_2O)_6 + \mathrm{Ru}_A^{2+}(H_2O)_6. \quad (8)$$

As shown in Fig. 2, for a given distance between two ruthenium metal centers, each hydrated Ru is one independent fragment in DFI. As such, it is natural to use FNE as the order parameter to drive the electron from one Ru to the other since the number of electrons in each fragment can be specified (*i.e.*, the electrons are naturally localized within fragments). Therefore, the free energy change of the full ET reaction such as eq. 7 can be obtained by TI,

$$\Delta A = -\int_0^1 \frac{\partial A(\eta)}{\partial \eta} d\eta = -\int_0^1 \left\langle \frac{\partial E^{DFI}(\eta)}{\partial \eta} \right\rangle_\eta d\eta = -\int_0^1 \left\langle \varepsilon^D_{\mathrm{HOMO}} - \varepsilon^A_{\mathrm{HOMO}} \right\rangle_\eta d\eta, \quad (9)$$

where $\varepsilon^D_{\mathrm{HOMO}}$ is the HOMO energy of fragment D and $\varepsilon^A_{\mathrm{HOMO}}$ is the HOMO energy of fragment A. Note that the HOMO becomes LUMO in fragment D at the finial state while the LUMO becomes HOMO in fragment A after the fractional electron is moved from fragment D to fragment A. *ΔA* vanishes in the specific self-exchange ET, but finite free energy differences are also allowed in this method for general cases.

By analyzing the sampled DFI-FNE trajectories, we can compute $\left\langle H_{DA}^2 \right\rangle$ and λ required in eq. 1 using the consistent DFI QM/MM energy expression without introducing any *ad hoc*

parameter. The reorganization energy λ can be readily evaluated by using the energy gap as the reaction coordinate.[19] For H_{DA}, we apply the fragment orbital approach combined with DFI. The frontier molecular orbitals for each fragment can be extracted and taken as the donor and acceptor orbital (i.e.,ϕ_D and ϕ_A) to compute H_{DA}[67],

$$H_{DA}=T_{DA}-S_{DA}\left(T_{DD}+T_{AA}\right)/2, \quad (10)$$

where $T_{DA}=\langle\phi_D|F\hat{\phi}_A\rangle$, $T_{DD}=\langle\phi_D|F\hat{\phi}_D\rangle$, $T_{AA}=\langle\phi_A|F\hat{\phi}_A\rangle$, and $S_{DA}=\langle\phi_D|\phi_A\rangle$. The operator $\hat{F}$ is the Fock operator that is constructed from the density of the entire system ρ without fragmentations. Total density ρ is the summation of converged fragmental densities ρ_D and ρ_A obtained from self-consistent DFI calculations. Note that our coupling calculations are similar to the FO-DFT used in a previous work.[39] However, the DFI frontier molecular orbitals are used here, rather than the CDFT wave functions,[39,40] to represent the two diabatic states for donor and acceptor, respectively. In order to obtain H_{DA} with consistent relative phases between donor and acceptor orbital, we adjust the signs of the donor and acceptor orbital, respectively, in each MD snapshot as the same as the signs in the first snapshot.

The Ru^{3+} and Ru^{2+} self-exchange ET process is simple but extremely challenging. Normal QM computations with both ions are even hardly converged due to electronic state degeneracy and delocalization errors of functionals.[68-70] Moreover, the ET rate constant of Ru^{3+} and Ru^{2+} self-exchange process requires the extensive sampling with different Ru^{3+} and Ru^{2+} distances. Hence, the final rate constant need to be computed and integrated as,[71]

$$k_{\text{total}}=\int_0^\infty 4\pi r^2 e^{-G(r)/k_B T}k_{ET}(r)\,dr, \quad (11)$$

where $G(r)$ is the potential of mean force for the two reactant complexes in solution that determines the pair distribution of the donor and acceptor. We will elucidate how DFI-FNE can be applied in this case and what are challenges in DFI-FNE.

3. Computational Details

The self-exchange redox couple $\mathrm{Ru}(H_2O)_6^{2+}-\mathrm{Ru}(H_2O)_6^{3+}$ was simulated by the DFI method with two individual fragments. The initial geometries of the two Ru complexes were built 10.0 Å apart, then solvated using TIP3P explicit solvent model in a cubic water box with the side length of 64 Å. A harmonic restraint was applied on the two Ru atoms with the equilibrium distance of 10.0 Å and the force constant of 100 kcal/mol/Å^2 . The separation distances were then sequentially reduced to 6.0 Å with the increment of 1.0 Å in a series of MD simulations that generated the initial geometries of Ru^{2+}–Ru^{3+} at different distances. Since the radius of the aqueous $Ru^{2+/3+}$ complexes are determined to be 5.5-6 Å, system with separation distance less than 6 Å would cause significant electronic coupling between the donor and acceptor, undermining the decoupled assumption in DFI. Thus, DFI calculations with separation distance less than 6 Å is avoided. The system was equilibrated for 16 ps with a timestep of 1 fs using the NVT ensemble, with a reduced restraining force constant of 10 kcal/mol/Å^2. In the following production MD, the simulation timescale is 16 ps for each separation distance, with 1000 snapshots recorded to compute the H_{DA} and reorganization energies. The DFI method with BLYP/LanL2DZ was used for the QM subsystem in the production MD, and BLYP/LanL2DZ(Ru)+6-31+G*(H_2O) was used in the calculation of H_{DA}. Classical MM MD umbrella samplings with force field parameters adapted from Ref.[34] were performed to obtain the potential mean force (PMF) of the Ru-Ru distance with a force cut-off of 16 Å combined with Particle Mesh Ewald method, since the

long range electrostatic interactions caused by periodic boundary condition (PBC) have not been incorporated in our QM/MM simulations. These long range interactions are important to compute the PMF profile for two ions.[44,72,73] In the PMF umbrella sampling, restraining potential of 5 kcal/mol/Å^2 were used to increase the overlap between sampling windows, generating an average of standard deviations of 0.35 Å for Ru-Ru distance. The window interval of 0.5 Å were used to cover the distances ranging from 5.5 Å to 16 Å and 160 ps MD was carried out for each window. Weighted histogram analysis method was used to reconstruct the PMF.[74]

4. Results and Discussion

4.1 Oxidation free energy

The absolute oxidation free energies were obtained by integrating the ensemble averages of eigenvalues of HOMO $\langle \varepsilon_{\mathrm{HOMO}} \rangle$ of the Ru complexes according to Eq. 6. Fig. 3 shows a profile of $\langle \varepsilon_{\mathrm{HOMO}} \rangle$ at different FNE of the Ru–Ru couple at the separation distance of 7.0 Å. The self-exchange ET reaction shows a symmetric profile of the two $\langle \varepsilon_{\mathrm{HOMO}} \rangle$ series. The integrations of the two curves generate the absolute oxidation free energies for the two fragments of 6.75 eV and 6.79 eV, with a difference of 0.04 eV. The average discrepancy of the oxidation free energy between the two self-exchange fragments is 0.03 eV over various separation distances, which is entirely due to the convergence in of the statistical sampling One may note that the absolute oxidation free energies of the aqueous Ru complex obtained in the full ET scheme are remarkably higher than that calculated in the half ET reaction (4.96 eV).[57] The shift of the oxidation free energies is mainly caused by the electrostatic field exerted by the second Ru complex in proximity. The presences of the two positively charged Ru complexes raise the electrostatic potential on each other thus make them stronger oxidizers. As shown in Fig. 4, we plot the oxidation free energies as a function of separation distance. The oxidation free energies decay from 7.05 eV at r = 6.0 Å to 6.50 eV at r = 10.0 Å, which fit well to the screened Coulomb potential shown in dashed line. Note that when long range electrostatic interactions are considered, the oxidation free energies may be lower.

4.2 Reorganization energy

The reorganization is a key factor that determines the rate constant and the mechanism of an ET process. Based on the DFI method, we can obtain the reorganization energy of the full ET process by projecting the diabatic free energy profiles over the energy gap similarly to the procedure in a half ET reaction.[57] The essential difference is that the energy gap of the full ET reaction is the energy difference between the swapped electronic states of the redox couple, i.e.

$$\Delta E = E\left[D(\mathrm{Ru}^{2+}) - A(\mathrm{Ru}^{3+})\right] - E\left[D(\mathrm{Ru}^{3+}) - A(\mathrm{Ru}^{2+})\right]. \quad (12)$$

Because the QM/MM electrostatic interaction cutoff is used in the DFI simulations, we investigated the influence of the choice of different cutoff radius on the final values of the reorganization energies. We chose two extreme separation distances, 6.0 Å and 10.0 Å to represent the two scenarios of close proximity and long ET distance. For each separation distance, the cutoff distance of 8.0 Å, 12.0 Å and 20.0 Å were examined and the corresponding reorganization energies are shown in Fig. 5. As we can see, the choice of the cutoff distance does not affect the reorganization energy of the Ru-Ru couple at close proximity while the electrostatic cutoff shows significant impact on the Ru-Ru couple at long distance. The increased separation distance between the two charged Ru complexes leads to disturbed solvent distributions in a larger region and thus requires larger QM/MM

interaction cutoff. Furthermore, a comparison of the reorganization energies of the five various separation distances between the choice of 12.0 Å and 20.0 Å cutoffs are shown in Fig. S2 and summarized in Table S2. Reorganization energies obtained using the cutoff of 20.0 Å generally show about 0.1 eV discrepancy compared to the results obtained using 12.0 Å. The λ convergence at 20.0 Å cutoff is also in agreement with our previous work on half ET reactions where detailed convergence tests were performed. Therefore, the cutoff distance is set to 20.0 Å in the production runs of DFI simulations.

The individual diabatic free energy profiles showing the reorganization energies at difference separation distances are plotted in Fig. S1, and the values of the reorganization energies are summarized in Table 1. In addition to the total reorganization energies, λ can also be decomposed to inner and outer shell reorganization energies by re-evaluating the sampled energies in the absence of solvent molecules.[57] As an example of Ru couple at r = 8.0 Å, the inner shell diabatic ET surfaces were constructed as shown in Fig. S3, which generates the inner shell reorganization energy of 0.69 eV. Based on the total reorganization energy of 3.13 eV, we can derive that the outer shell contribution is 2.44 eV, which is the major part of the reorganization energy in the Ru^{2+}-Ru^{3+} self-exchange ET reaction. This suggests that the outer shell reorganization plays important roles to determine the total reorganization energy since two hydrated ions are rigid during ET.

We noticed that the reorganization energies calculated using our QM/MM method are consistently overestimated.[57] In the comparison of other simulations on the same self-exchange process, we find that the lack of polarizable solvent model is an important reason for the overestimation.[20,24,34] The simulations with solvent polarization generate relatively lower and more accurate reorganization energies.[36,37,41] In addition, the lack of PBC in QM calculations may also contribute to the error in the reorganization energies. Since the reorganization energy has an exponential dependence on ET rate k_{ET} (for self-exchange reactions with zero redox free energy), we here rescaled the reorganization energy to reduce the errors due to the lack of solvent polarization and PBC with the scaling coefficient 0.63, which was the determined from the ratio of the reorganization energy of a single Ru complex (2.45 eV) from our previous work[57] to the experimental estimation (1.54 eV).[12]

4.3 Electronic coupling

To calculate the ET rate, the electronic coupling H_{DA} needs to be determined. According to our DFI scheme, we computed the electronic coupling using the fragment orbital approximation (Eq. 10). Since the calculation of H_{DA} involves the molecular orbital overlap S_{DA}, we examined the basis set dependence of S_{DA}. The basis set LanL2DZ is used in the direct MD sampling to achieve affordable cost for the “on-the-fly” DFI-FNE/MM calculations. Based on the MD trajectories, we re-evaluated the S_{DA} of each snapshots using larger basis sets, 6-31+G* and 6-31++G**. The comparison of $|S_{DA}|$ among different basis sets is shown in Fig. 6. The other two large basis sets show good agreement with each other, indicating the convergence of the size of the basis set; however, the small basis set LanL2DZ is obviously not sufficient to calculate accurately the orbital overlap S_{DA} and the electronic coupling H_{DA}. As such, we choose the 6-31+G* in the calculations of H_{DA} to balance the computational cost and the accuracy. In addition, we analyzed S_{DA} in different ET reaction regions by comparing the ensemble averages of S^2_{DA} obtained from samplings at different electronic states as shown in Fig. 7. Based on the conformational trajectories of reactant and product states, the values of $\langle S^2_{DA} \rangle$ at the reaction endpoints are about 10^{-9}, which is one order of magnitude smaller than the ensemble averages obtained for the diabatic transition state ($\sim 10^{-8}$) where $\Delta E < 0.05$ eV. Although the FNE state with even distribution of electron on donor and acceptor ($Ru^{2.5+}$–$Ru^{2.5+}$) restrains the system near the transition state ($\langle \Delta E \rangle$=0.002 eV), it still allows thermal fluctuations of the solvent dynamics

and shows standard deviation of ΔE to be 0.37 eV. Therefore the ensemble of $Ru^{2.5+}$–$Ru^{2.5+}$ is not the strict diabatic transition state ensemble (defined as $|\Delta E| < 0.05$ eV). Interestingly, as shown in Fig. 7, the statistics of $\langle S^2_{DA} \rangle$ are almost identical for the two ensembles, indicating that the FNE state is a good approximation to the diabatic ET transition state.

Strictly, the electronic coupling H_{DA} between the donor and acceptor fragments should also be computed at the transition states, the cross region where the energy gap is zero. Thus, only the snapshots with the energy gaps less than 0.05 eV were used to compute the ensemble averages of H_{DA}. The final values of H_{DA} for Ru couple at different separation distances were summarized in Table 1. The distance dependence of H_{DA} was analyzed and fitted to exponential distance dependence$|H_{DA}| = A\exp[-\beta r/2]$, with the distance decay constant $\beta/2 = 1.16$ Å^{-1}, as shown in Fig. 8. Previous simulations on the same ET process reported similar values and distance dependent decay rate of H_{DA}.[37] The distance decay rate constant in our simulations agrees with the estimation in aqueous Fe^{2+}–Fe^{3+} self-exchange ($\beta/2$=12 Å^{-1}),[71] and it is significantly larger than those in protein environments ($\beta/2 = 0.55$ Å^{-1}).[75] This is not surprising because the Ru^{2+}–Ru^{3+} self-exchange in aqueous solution does not have a specific “bridge” but dynamic water molecules that mediate the ET,[76] hence the ET rate decays much faster when the separation distance increases.

4.4 ET rate k_{ET} and total reaction rate k of Ru^{2+}–Ru^{3+} self-exchange

With the redox free energy ΔG, the reorganization energy λ and the electronic coupling H_{DA} obtained individually, we can calculate the ET rate k_{ET} according to Eq. 1. The values of k_{ET} calculated using both the native and rescaled reorganization energies at different separation distances were summarized in Table 1. The ET rates k_{ET} are greatly promoted using the rescaled reorganization energies. With all the distance dependences, we can finally compute the total reaction rate k by integrating the ET rate k_{ET} over the space following Eq. 11, where k_{ET} are averaged with the Ru–Ru pair distribution $e^{-G(r)/kBT}$ at the corresponding separation distance. The distance dependence of the intermolecular interactions $G(r)$ sampled by classical MD simulations is shown in Fig. 9. The intermolecular interactions $G(r)$ agrees with a previous simulation results[37] and fits nicely the screened Coulomb potential shown in dashed line. The baseline of $G(r)$ was offset to zero at $r=\infty$. Spherical integration of the weighted k_{ET} generates the total rate constant of the self-exchange ET reaction between Ru^{2+}-Ru^{3+} couple as $k = 0.11$ M^{-1} S^{-1} . Before we can directly compare the computed rate constant to experimental measurements, the effect of nuclear tunneling over the activation barrier and the ionic strength must be considered. In the aqueous Fe^{2+}–Fe^{3+} self-exchange, the nuclear tunneling introduces a rate enhancement factor of about 10,[2,22,34] based on different water models. This increases the total rate constant k for about one order of magnitude. In addition, the high ionic concentration in acidic solution may increase the measured ET rate. The overall effect of finite ionic strength (5M) was reported to promote the rate by about two orders of magnitude compared to infinite dilution limit.[37] Considering the $\sim 10^3$ enhancement due to the quantum tunneling and ionic strength, the total rate of 0.11 M^{-1} S^{-1} in our simulation is scaled to 1×10^2 and shows good agreements with the experimental observation of 20 M^{-1} s^{-1}.[77]

5. Conclusions

In this work, we developed the DFI-FNE QM/MM approach to study the full ET reaction. The new method allows us to calculate the redox free energies and reorganization energies of the donor and acceptor simultaneously and generates the redox free energy and diabatic free energy surface of the full ET reaction. Combined with fragment-orbital approach, the electronic couplings between the donor and acceptor can be readily computed by the DFI scheme. As such, the absolute the ET rate constant k_{ET} can be obtained without introducing

ad hoc parameters using DFI-FNE. This approach should have significant impact on computing the ET rate constants for chemical and biological systems.

To further improve the accuracy, the long-range electrostatic interactions need to be considered. In addition, how to improve the solvent description is also important to obtain accurate reorganization energy. For instance, the MM model in DFI-FNE QM/MM significantly overestimates λ. More importantly, many other factors in electrochemical experiments, e.g. pH dependence, ion strength, interfacial effects, can prevent good agreement between theoretical predictions and experimental measurements. The difference between physiological environment and *in vitro* experiments introduce further complications in understandings of many important biochemical ET reactions. Further studies related to these issues will be investigated in our group.

Supplementary Material

Refer to Web version on PubMed Central for supplementary material.

Acknowledgments

Supports from the National Institute of Health (NIH R01-GM061870 to W.Y.; P50GM067082 to X. H.) are greatly appreciated. X. H. thanks to the UNC EFRC: Solar Fuels and Next Generation Photovoltaics, an Energy Frontier Research Center funded by the U.S. Department of Energy, Office of Science, Office of Basic Energy Sciences under Award Number DE-SC0001011. X.H. thanks the 2010 HPC Advisory Council University Award and personally thanks the helps from Pak Lui. We thank Prof. Spiros S. Skourtis for his helpful comments. We also thank KillDevil computing resources at UNC.

References

1. Marcus RA, Sutin N. Biochimica et Biophysica Acta (BBA) - Reviews on Bioenergetics. 1985; 811:265.
2. Song X, Marcus RA. J Chem Phys. 1993; 99:7768.
3. Han P, Xu RX, Li B, Xu J, Cui P, Mo Y, Yan. J Phys Chem B. 2006; 110:11438. [PubMed: 16771417]
4. Newton MD, Sutin N. Annu Rev Phys Chem. 1984; 35:437.
5. Hopfield JJ, Onuchic JN, Beratan DN. Science. 1988; 241:817. [PubMed: 17829175]
6. Beratan DN, Betts JN, Onuchic JN. Science. 1991; 252:1285. [PubMed: 1656523]
7. Onuchic JN, Beratan DN, Winkler JR, Gray HB. Annu Rev Biophys Biomol Struct. 1992; 21:349. [PubMed: 1326356]
8. Beratan DN, Onuchic JN, Betts JN, Bowler BE, Gray HB. J Am Chem Soc. 1990; 112:7915.
9. Beratan D, Onuchic J, Winkler, Gray H. Science. 1992; 258:1740. [PubMed: 1334572]
10. Brown GM, Sutin N. J Am Chem Soc. 1979; 101:883.
11. Brunschwig BS, Logan J, Newton MD, Sutin N. J Am Chem Soc. 1980; 102:5798.
12. Brunschwig BS, Creutz C, Macartney DH, Sham TK, Sutin N. Faraday Discussions of the Chemical Society. 1982; 74:113.
13. Ratner MA. J Phys Chem. 1990; 94:4877.
14. Mujica V, Kemp M, Ratner MA. J Chem Phys. 1994; 101:6849.
15. Davis WB, Wasielewski MR, Ratner MA, Mujica V, Nitzan A. J Chem Phys A. 1997; 101:6158.
16. Segal D, Nitzan A, Davis WB, Wasielewski MR, Ratner MA. J Chem Phys B. 2000; 104:3817.
17. Senthilkumar K, Grozema FC, Guerra CF, Bickelhaupt FM, Lewis FD, Berlin YA, Ratner MA, Siebbeles LDA. J Am Chem Soc. 2005; 127:14894. [PubMed: 16231945]
18. Milischuk AA, Matyushov DV, Newton MD. Chem Phys. 2006; 324:172.
19. Warshel AJ. Phys Chem. 1982; 86:2218.

20. Kuharski RA, Bader JS, Chandler D, Sprik M, Klein ML, Impey RW. J Chem Phys. 1988; 89:3248.
21. Zichi DA, Ciccotti G, Hynes JT, Ferrario M. J Phys Chem. 1989; 93:6261.
22. Bader JS, Kuharski RA, Chandler D. J Chem Phys. 1990; 93:230.
23. Gehlen JN, Chandler D, Kim HJ, Hynes JT. J Phys Chem. 1992; 96:1748.
24. Ando K. J Chem Phys. 2001; 114:9470.
25. Ungar LW, Newton MD, Voth GA. J Chem Phys B. 1999; 103:7367.
26. Li G, Zhang X, Cui Q. J Chem Phys B. 2003; 107:8643.
27. Olsson MHM, Hong G, Warshel A. J Am Chem Soc. 2003; 125:5025. [PubMed: 12708852]
28. Blumberger J, Bernasconi L, Tavernelli I, Vuilleumier R, Sprik M. J Am Chem Soc. 2004; 126:3928. [PubMed: 15038747]
29. Blumberger J, Sprik M. J Phys Chem B. 2005; 109:6793. [PubMed: 16851765]
30. Blumberger J, Klein ML. J Am Chem Soc. 2006; 128:13854. [PubMed: 17044714]
31. Blumberger J, Tavernelli I, Klein ML, Sprik M. J Chem Phys. 2006; 124:064507.
32. Blumberger J. Phys Chem Chem Phys. 2008; 10:5651. [PubMed: 18956100]
33. Blumberger J. J Am Chem Soc. 2008; 130:16065. [PubMed: 19032099]
34. Blumberger J, Lamoureux G. Mol Phys. 2008; 106:1597.
35. Seidel R, Faubel M, Winter B, Blumberger J. J Am Chem Soc. 2009; 131:16127. [PubMed: 19831354]
36. Oberhofer H, Blumberger J. J Chem Phys. 2009; 131:064101. [PubMed: 19691372]
37. Oberhofer H, Blumberger J. Angewandte Chemie International Edition. 2010; 49:3631.
38. Tipmanee V, Oberhofer H, Park M, Kim KS, Blumberger J. J Am Chem Soc. 2010; 132:17032. [PubMed: 21053902]
39. Oberhofer H, Blumberger J. J Chem Phys. 2010; 133:244105. [PubMed: 21197974]
40. Oberhofer H, Blumberger J. Phys Chem Chem Phys. 2012
41. Sit PHL, Cococcioni M, Marzari N. Phys Rev Lett. 2006; 97:028303. [PubMed: 16907484]
42. Cascella M, Magistrato A, Tavernelli I, Carloni P, Rothlisberger U. Proc Natl Acad Sci U S A. 2006; 103:19641. [PubMed: 17179046]
43. Improta R, Barone V, Newton MD. ChemPhysChem. 2006; 7:1211. [PubMed: 16680796]
44. Sulpizi M, Raugei S, VandeVondele J, Carloni P, Sprik M. J Chem Phys B. 2007; 111:3969.
45. Kamerlin SCL, Haranczyk M, Warshel A. J Chem Phys B. 2008; 113:1253.
46. Cheng J, Sulpizi M, Sprik M. J Chem Phys. 2009; 131:154504. [PubMed: 20568869]
47. Costanzo F, Sulpizi M, Valle RGD, Sprik M. J Chem Phys. 2011; 134:244508. [PubMed: 21721644]
48. Sutin N. Acc Chem Res. 1982; 15:275.
49. Newton MD. Chem Rev (Washington, DC, U S). 1991; 91:767.
50. Warshel A, Parson WW. Annu Rev Phys Chem. 1991; 42:279. [PubMed: 1747189]
51. Barbara PF, Meyer TJ, Ratner MA. J Phys Chem. 1996; 100:13148.
52. Gray HB, Winkler JR. Annu Rev Biochem. 1996; 65:537. [PubMed: 8811189]
53. Nitzan A. Annu Rev Phys Chem. 2001; 52:681. [PubMed: 11326078]
54. Beratan DN, Skourtis SS, Balabin IA, Balaeff A, Keinan S, Venkatramani R, Xiao D. Acc Chem Res. 2009; 42:1669. [PubMed: 19645446]
55. Skourtis SS, Waldeck DH, Beratan DN. Annu Rev Phys Chem. 2010; 61:461. [PubMed: 20192814]
56. Wu Q, Van Voorhis T. J Chem Theory Comput. 2006; 2:765.
57. Zeng X, Hu H, Hu X, Cohen AJ, Yang W. J Chem Phys. 2008; 128:124510. [PubMed: 18376946]
58. Hu H, Lu Z, Yang W. J Chem Theory Comput. 2007; 3:390. [PubMed: 19079734]
59. Hu H, Lu Z, Parks JM, Burger SK, Yang W. J Chem Phys. 2008; 128:034105. [PubMed: 18205486]
60. Zeng X, Hu H, Hu X, Yang W. J Chem Phys. 2009; 130:164111. [PubMed: 19405565]

61. Fujimoto K, Yang W. J Chem Phys. 2008; 129:054102. [PubMed: 18698883]
62. Hu X, Jin Y, Zeng X, Hu H, Yang W. Phys Chem Chem Phys. 2012
63. Yang W. Phys Rev Lett. 1991; 66:1438. [PubMed: 10043209]
64. Yang W. Phys Rev A. 1991; 44:7823. [PubMed: 9905920]
65. Parr, RG.; Yang, W. Density-Functional Theory of Atoms and Molecules. Oxford University Press; New York: 1989.
66. Cohen AJ, Mori-Sánchez P, Yang W. Physical Review B. 2008; 77:115123.
67. Kubar T, Woiczikowski PB, Cuniberti G, Elstner M. J Chem Phys B. 2008; 112:7937.
68. Mori-Sánchez P, Cohen AJ, Yang W. Phys Rev Lett. 2008; 100:146401. [PubMed: 18518055]
69. Cohen AJ, Mori-Sánchez P, Yang W. Science. 2008; 321:792. [PubMed: 18687952]
70. Cohen AJ, Mori-Sánchez P, Yang W. Chem Rev (Washington, DC, U S). 2011; 112:289.
71. Logan J, Newton MD. J Chem Phys. 1983; 78:4086.
72. Darden T, York D, Pedersen L. J Chem Phys. 1993; 98:10089.
73. Laino T, Mohamed F, Laio A, Parrinello M. J Chem Theory Comput. 2005; 1:1176.
74. Kumar S, Rosenberg JM, Bouzida D, Swendsen RH, Kollman PA. J Comput Chem. 1992; 13:1011.
75. Gray HB, Winkler JR. Proc Natl Acad Sci U S A. 2005; 102:3534. [PubMed: 15738403]
76. Lin J, Balabin IA, Beratan DN. Science. 2005; 310:1311. [PubMed: 16311331]
77. Bernhard P, Helm L, Ludi A, Merbach AE. J Am Chem Soc. 1985; 107:312.

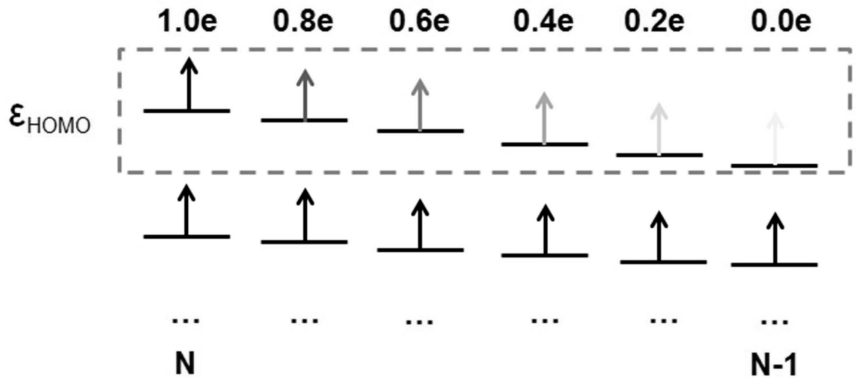

Figure 1.
Schematic view of FNE procedure.

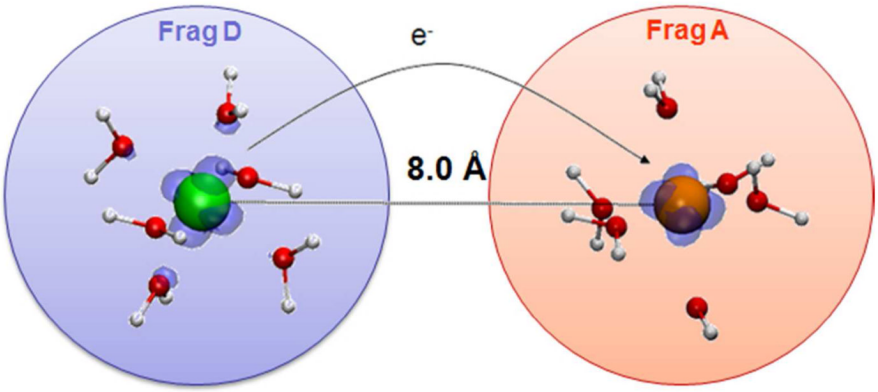

Figure 2.
Schematic view of DFI-FNE procedure for the Ru^{2+}-Ru^{3+} self-exchange ET process.

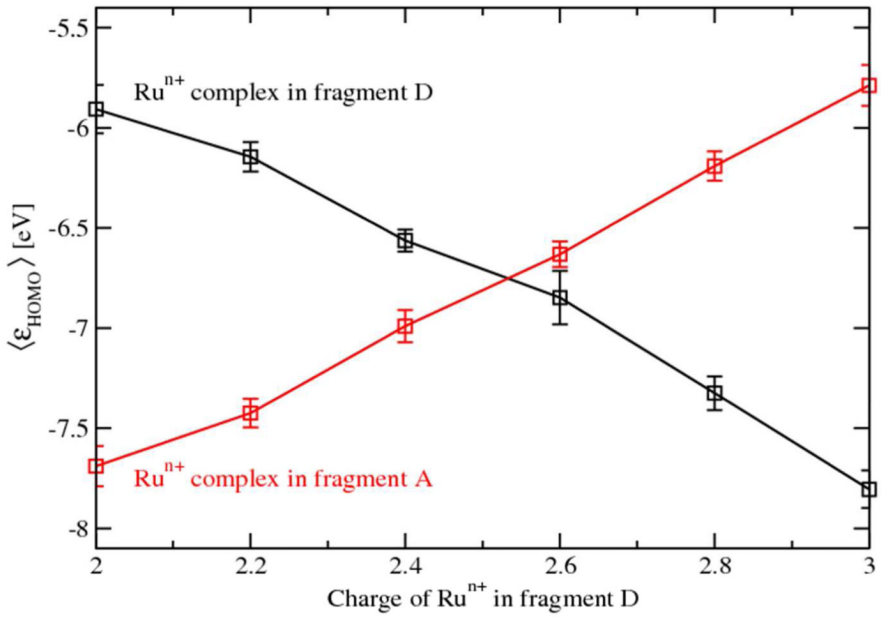

Figure 3.

Symmetrical redox profile of the self-exchange ET reaction (Ru – Ru distance of 7.0 Å is shown). Values of $<\varepsilon_{HOMO}>$ are obtained in DFI simulations and the error bars show the statistic uncertainties. Integration of each $<\varepsilon_{HOMO}>$ curve generates the oxidation free energy of the corresponding Ru complex.

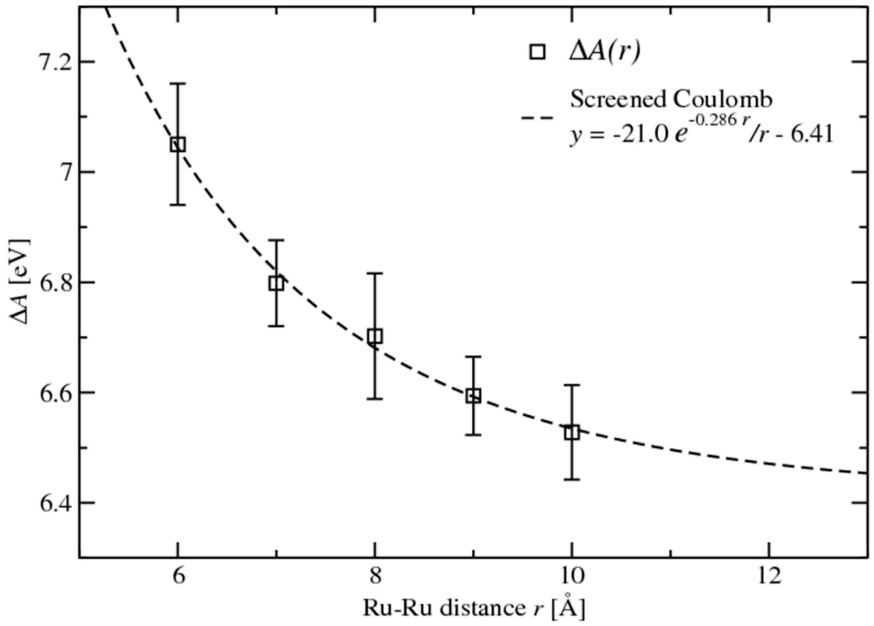

Figure 4.

Distance dependence of oxidation free energies of Ru complexes. The calculated results are shown in black square with error bars showing the sampling uncertainties, and the dashed line is fitted to screened Coulomb potential.

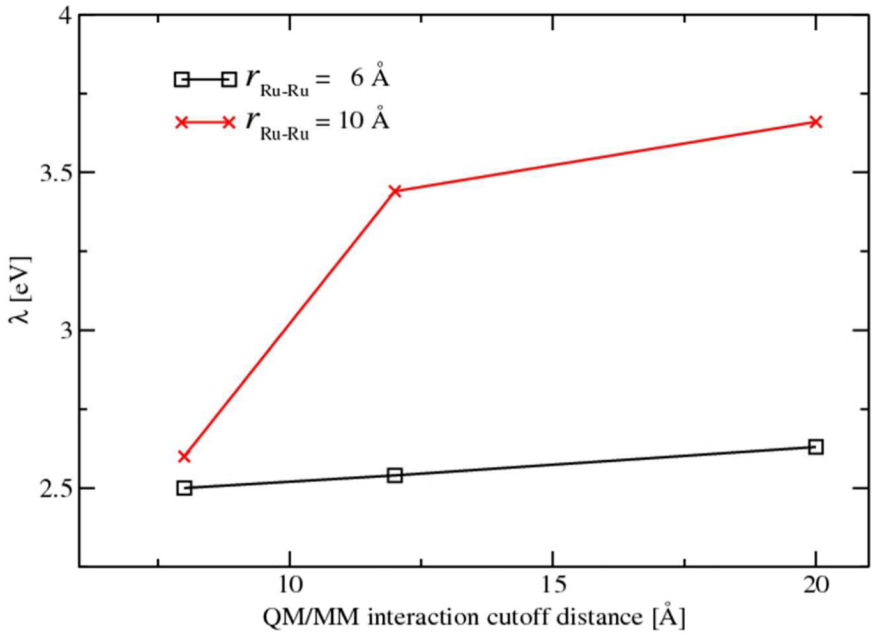

Figure 5.
Influence of QM/MM electrostatic cutoff distance on reorganization energies.

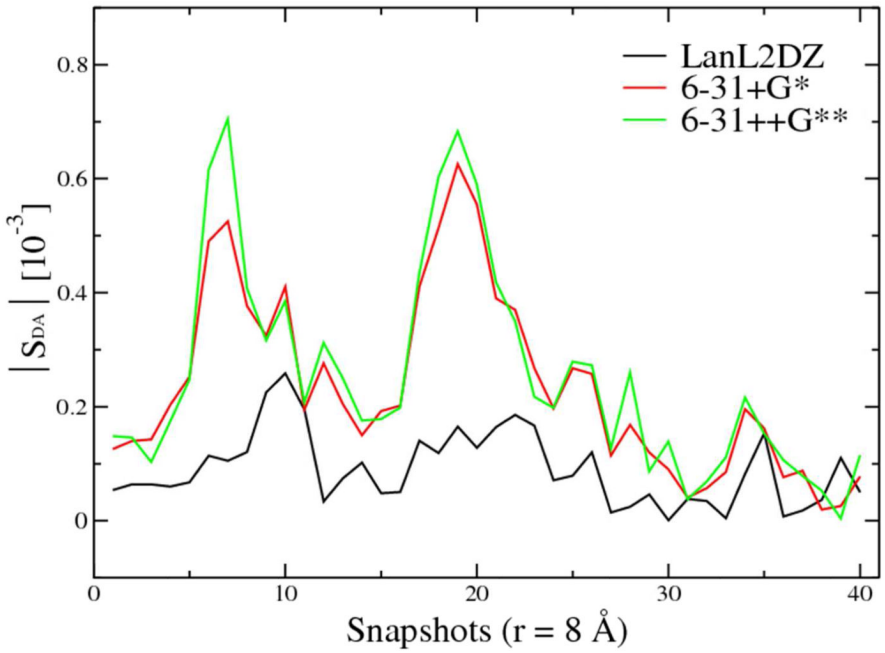

Figure 6.
Basis set dependence of $|S_{DA}|$ using LanL2DZ, 6-31+G*, and 6-31++G**. Convergence is achieved at 6-31+G*.

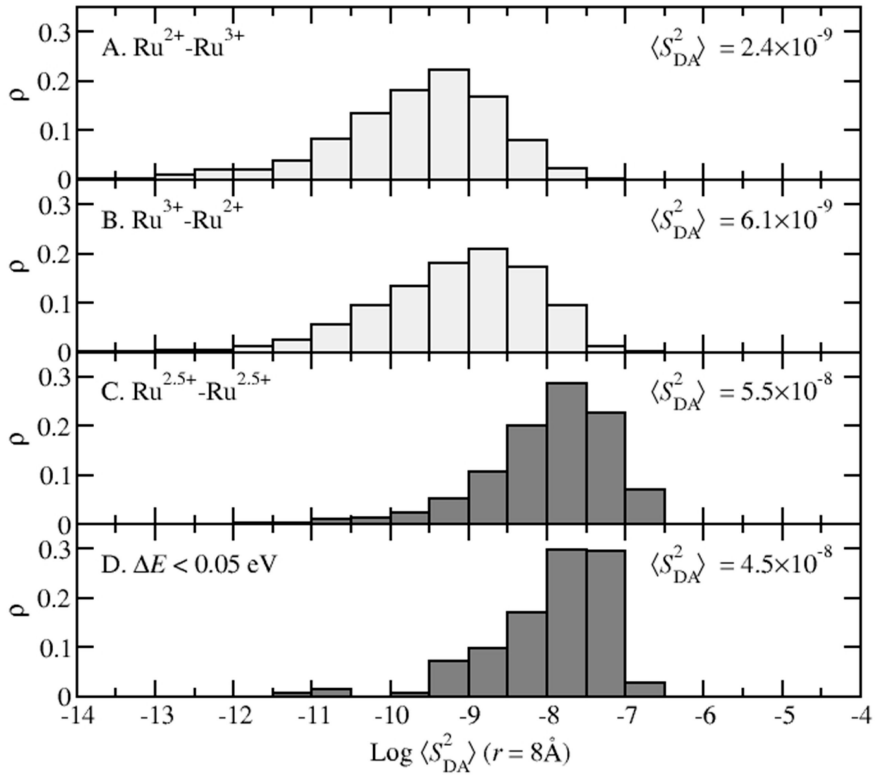

Figure 7.

Distribution of $<S^2_{DA}>$ in various electronic states: A. reactant state (light gray); B. product state (light gray); C. adiabatic FNE state with even electron distribution (dark gray); D. diabatic transition state with energy gap criterion of ΔE<0.05 eV (dark gray). Ensemble average value of $<S^2_{DA}>$ show about one order of magnitude increase in the transition state compared to the reactant or product state.

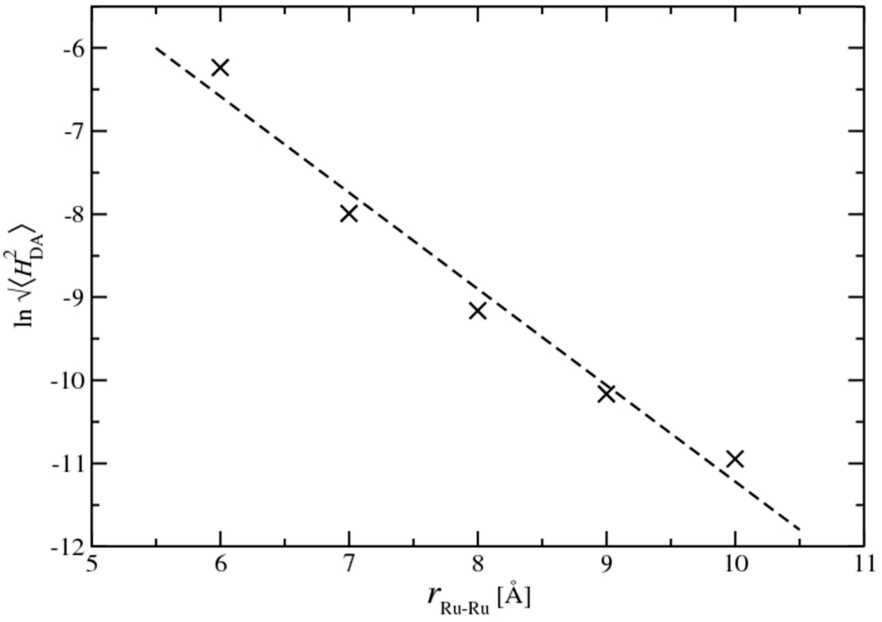

Figure 8.

Distance dependence of H_{DA} (black cross). Linear regression (dashed-line) generates the slope of 1.16, which leads to the decay constant β of 2.32 $Å^{-1}$. (6-31+G* basis set is used to calculate H_{DA}.)

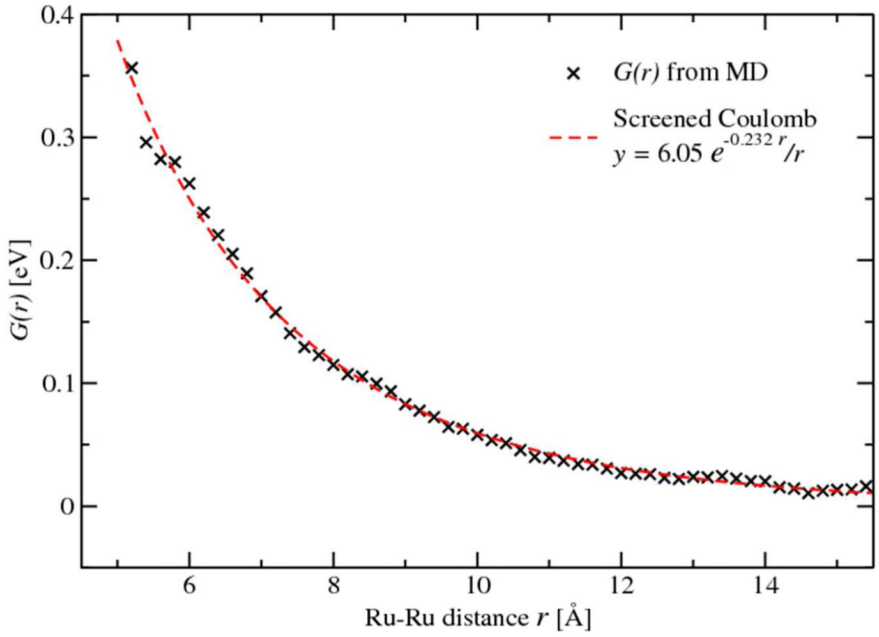

Figure 9.
PMF along Ru-Ru distance from classic MD simulations. Simulation results of the Ru–Ru interaction (black cross) behave like a screened Coulomb potential (fitted as red dashed-line).

Table. 1

Reorganization energies, H_{DA} and k_{ET} at different Ru-Ru distance

r/Å	$\langle H^2_{DA}\rangle^{1/2}$/eV	$\lambda(r_{cutoff}$=20 Å)/eV	k_{ET}/M^{-1}s^{-1}	λ_{scaled}/eV	k_{ET} (λ_{scaled})/s^{-1}[a]
6.0	2.03E-03	2.63	3.81E-01	1.66	5.88E+03
7.0	3.33E-04	2.97	3.59E-04	1.87	1.87E+01
8.0	1.07E-04	3.23	2.89E-06	2.03	3.80E-01
9.0	3.75E-05	3.40	6.71E-08	2.14	1.62E-02
10.0	1.66E-05	3.66	1.02E-09	2.31	6.28E-04

[a]The free energy difference of the self-exchange process (ΔA) is rounded to zero in the calculations of k_{ET}.